JOURNAL OF MATERIALS SCIENCE 20 (1985) 955–966

Thermal wave testing of plasma-sprayed coatings and a comparison of the effects of coating microstructure on the propagation of thermal and ultrasonic waves

P. M. PATEL, D. P. ALMOND
School of Materials Science, University of Bath, Claverton Down, Bath, Avon, UK

A thermal wave technique for the non-destructive examination of plasma-sprayed coatings is described. Measurements of molybdenum NiAl and aluminium coatings are presented to demonstrate that the technique can be used for defect detection, coating thickness determination and thermal property evaluation. The effects observed are shown to be attributable to thermal wave interference in the coating material. A semi-quantitative model of the coating microstructure is presented to compare its effects on the propagation of ultrasonic and thermal waves. The model predicts the coating material's very high attenuation of ultrasonic waves and a very low attenuation for thermal waves. This is taken to explain the success of thermal waves, and the failure of ultrasonic waves, in producing measurable interference effects in plasma-sprayed coatings.

1. Introduction

Thermal spray coatings are becoming increasingly important in many high technology industries for the production of the specific surface properties required by engineering components [1]. Coatings are sprayed for wear or corrosion resistance, thermal or electrical insulation, reclamation of worn machine parts and for conservation of expensive raw materials. Hard surface coatings of tungsten carbide/chromium carbide are currently used for their good wear resistance characteristics. Materials such as aluminium are being flame sprayed to provide protection from environmental corrosion. Coatings of M-CrAlY (where M is nickel, cobalt or iron) and zirconium oxide are being applied to afford resistance to the hot corrosive environments found in gas turbines. Ceramic coatings (e.g. alumina) are becoming widely used for their electrical and thermal insulation properties.

The quality assurance of thermally sprayed coatings is currently hampered by the absence of a satisfactory non-destructive testing technique. A technique is needed that will determine the integrity (i.e. the presence of coating delaminations or adhesion defects) and the thickness of a coating on a component. At present, stringent quality control practices and in-service tests are employed to ensure that a given coating meets specified requirements. Some of the prerequisites of a suitable non-destructive inspection technique can be formulated as those satisfying the following criteria:

1. being non-contactive and non-destructive;
2. providing thickness determination and defect detection;
3. being applicable to the wide range of geometrical configurations found in engineering components.

These requirements would seem to be met by a suitable interferometric technique. Such a technique necessitates the use of a wave which will propagate, relatively unattenuated, through a thickness (typically 200 μm) of coating material.

0022–2461/85 $03.00 + .12

Optical interference is obviously impossible as the materials usually sprayed are opaque. Ultrasonic wave interference is not generally observed in these coatings [2] because of the high attenuation of these waves by sprayed coating material. Cox *et al.* [2] reported an attenuation of ~ 500 dB cm^{-1} and showed that this prevented the formation of ultrasonic interference effects. Green [3] and Luukkala [4] have demonstrated that thermal waves may be used for the testing of sprayed coatings and Busse and Eyerer [5] have shown them to be of value for the examination of polymeric coatings. In this paper we show that these thermal waves exhibit the required interference phenomena in thermal sprayed coatings. In order to understand the success and failure of thermal and ultrasonic waves, it is necessary to examine the effect of coating microstructure on the propagation of these two types of wave.

Coating microstructure is described in the next section; this is followed by a discussion of thermal waves and experimental results which demonstrate interference effects in sprayed coatings. Finally, a semiquantitative analysis is presented to explain the differences in the effects of coating microstructure on the propagation of ultrasonic and thermal waves.

2. Coating microstructure

The deposition of plasma-sprayed coatings can be divided into two stages: (1) the melting of the coating material in the high-temperature (10 000 K) plasma arc flame; (2) the subsequent projection of the molten particles in a high-velocity gas stream (N_2/Ar) towards a roughened substrate. The required coating thickness is built up by a succession of passes of the substrate through the spray. This mode of deposition generally introduces porosity, cracks, delaminations and fluctuations in coating thickness. Fig. 1 shows, schematically, some of the typical microstructural features observed in optical and scanning electron micrographs of plasma-sprayed coatings and other thermally sprayed coatings. Table I summarizes these features; actual micrographs of some coating structures can be found in the references given

TABLE I A tabulation of the typical microstructural features observed in thermally sprayed coatings

Microstructural features	Reference
Finite porosity. Spherical pores (1 μm), very thin elongated pores (0.01 to 0.1 μm), formed by volume shrinkage and microcracking under thermal stresses	[6, 7]
Layered arrangements of coating material. Layers separated by the thin elongated pores. Very fine grain structure in these solidified coating layers	[8]
Random areas of contact between these coating layers	[8]
Possibility of metastable phases, e.g. Al_2O_3	[6, 7]
A thin amorphous structure very near the coating substrate interface	[9, 10]
Variation in grain structure from columnar near the coating/substrate interface to equiaxed near the surface	[11]

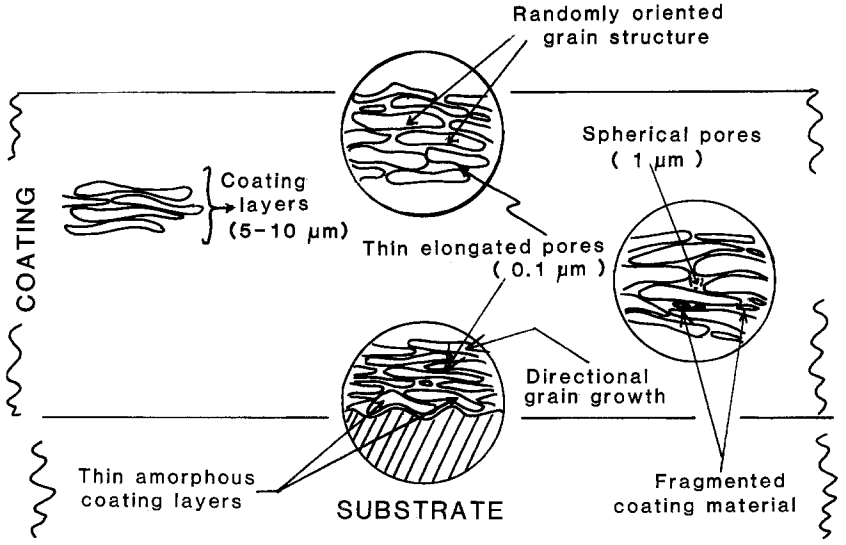

Figure 1 A schematic representation of some typical microstructural features found in thermally sprayed coatings.

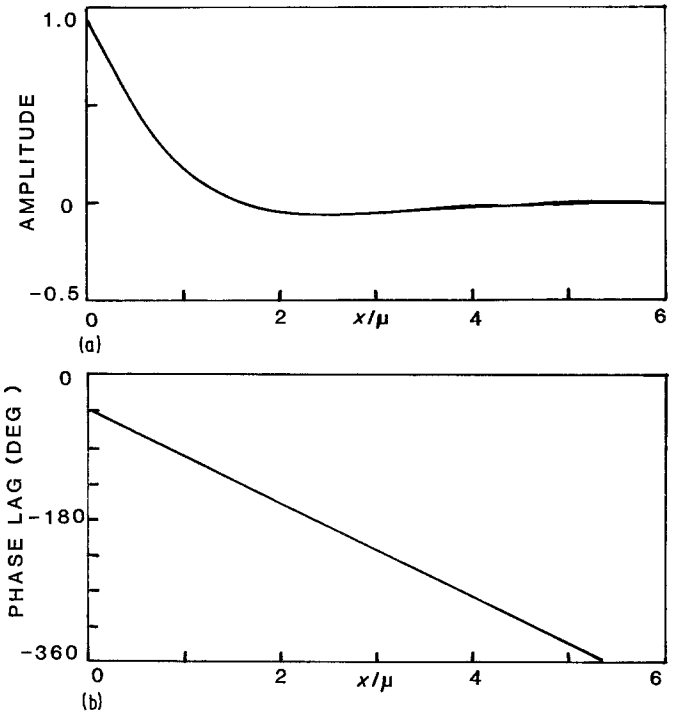

Figure 2 (a) and (b) The amplitude and phase variation of the thermal wave with the parameter x/μ, at time instant $\omega t = 0$.

in the table. The formation of these features is inherent to the solidification process which is essentially a very rapid cooling of molten spherical particles of the coating material and the flattening of these droplets as they strike the substrate. Cooling rates of $10^{6°}\,C\,sec^{-1}$ are easily attained by this deposition method.

3. Thermal waves

Currently, there is an increasing interest in optically generated thermal waves due to the development of techniques such as photoacoustic spectroscopy [12] and photoacoustic microscopy [13]. Previously non-optical methods of thermal-wave generation have been used for thermal diffusivity [14, 15] and coating-thickness measurements [3].

When a periodic heat source is applied to the surface of a sample (e.g. from a modulated light beam or a periodically heated resistor), this leads to a temperature modulation that propagates into the sample as a heavily damped wave, a thermal wave. Equation 1 [16] represents mathematically, a one-dimensional thermal wave, of angular frequency ω, propagating in the positive x-direction, see Fig. 2a.

$$T(x, t) = T_0\, e^{-x/\mu}\, e^{j(\omega t - x/\mu)} \qquad (1)$$

where $j = (-1)^{1/2}$, $\omega = 2\pi f$, f is the modulation frequency, $\mu = (2\alpha/\omega)^{1/2} = (\alpha/\pi f)^{1/2}$; the thermal diffusion length, and α is the thermal diffusivity. It can be seen from Equation 1 that the amplitude of the thermal wave, $T(x, t)$, decreases exponentially with distance, x, into the sample. The thermal diffusion length, μ, is the distance over which the magnitude of the thermal wave decays to $1/e$ of its initial value, T_0, and its phase changes by one radian (57°). Fig. 2b shows the phase angle variation with x/μ. This figure illustrates that the phase angle depends only on the physical and thermal properties of the sample. A useful feature of a thermal wave is that its decay rate, μ, can be controlled by varying the modulation frequency. This provides a depth profiling capability [17, 18] for probing solid matter, see Fig. 3a.

Thermal waves will undergo reflection or scattering processes when they encounter regions of different thermal characteristics [19], (see Fig. 3b); in the same way as electromagnetic or ultrasonic waves at regions of different refractive index or acoustic impedance. This, and their wave-like properties, suggest that thermal waves might be used as an alternative waveform for performing interferometry in thin coatings. To observe such interference effects in a coating the thermal wavelength must be comparable to coating thickness and the wave must suffer little attenuation in its passage through the coating material.

The surface temperature of a sample, exposed

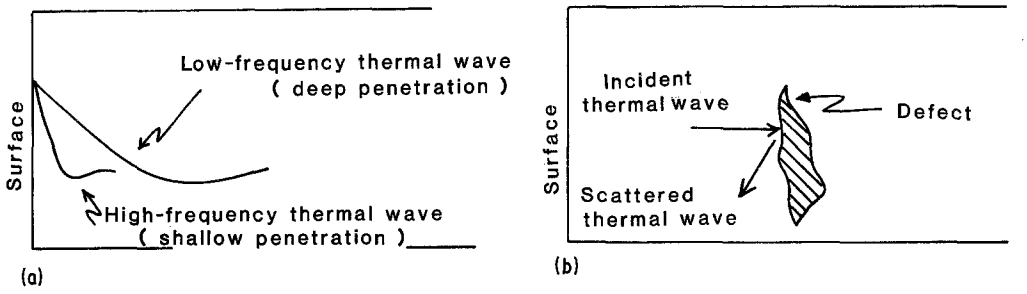

Figure 3 (a) A schematic illustration of the depth probing nature of low- and high-frequency thermal waves. (b) Thermal wave scattering from a region of different thermal characteristics in the path of the propagating wave.

to a modulated light source, will be dependent on, (1) the optical and thermal properties of the sample, and (2) the effects of sample geometry on heat flow. Bennet and Pattey [20] have analysed thermal wave interference in a coating on a thermally thick substrate. Their general expression for resultant surface temperature reduces to:

$$\phi_s = \frac{(1-r)I_0}{k\sigma}\left[\frac{1+Re^{-2\sigma L}}{1-Re^{-2\sigma L}}\right] \qquad (2)$$

for metallic coatings, where the optical absorption depth, $1/\beta$, is very small $\lesssim 0.1\ \mu m$; the skin depth. In the above expression I_0 is the incident optical intensity, r is the optical reflection coefficient of the surface, L is the coating thickness and k is its thermal conductivity, σ is the complex thermal wave vector, and R is the thermal wave reflection coefficient for the coating substrate interface. R is given by

$$R = (1-b)/(1+b) \qquad (3)$$

where

$$b = \left[\frac{(\rho ck)_b}{(\rho ck)_s}\right]^{1/2} \qquad (4)$$

ρ is the density, c the specific heat capacity, and subscripts s and b refer to the surface coating and backing (substrate) materials, respectively.

Figs. 4a and b show the changes in signal and phase, caused by the interference effects, plotted against the thermal thickness, *asL*. *as* is given by $(1/\mu)$ and is related to σ by

$$\sigma = (1+j)as \equiv (1+j)\frac{1}{\mu}. \qquad (5)$$

A variety of techniques can be used [21–23] to observe thermal wave interference effects. In this study, photothermal radiometry, PTR [23], was chosen because it is a simple non-contactive technique satisfying the requirements mentioned in Section 1. In PTR the changes in surface temperature are detected by an infrared detector. A practical problem [24] is that variations in the surface reflectivity, that might be caused by unimportant marks or blemishes, can affect the amount of the light that is absorbed and, as a result, the amplitude of the detected signal. The phase of the signal, given by the term in square brackets in Equation 2, will be unaffected by the variation in the amount of absorbed optical energy. For this reason we will concentrate on the changes in the phase angle of the detected signal. The dependence of phase angle on coating thickness and the presence of adhesion defects is outlined below and illustrated in Fig. 5.

3.1. Thickness change

Thermal wave interference produces changes in the phase of the detected signal which depend on the wave number and the coating thickness, *asL*, as has been illustrated in Fig. 4b. The magnitude of the phase change varies with both the particular *asL* value, determined by the modulation frequency, and the coating substrate reflection coefficient. Thus part or all of a locus of the type shown in Fig. 4b will be traced by phase-angle measurements of coatings of varying thicknesses (Fig. 5a). This provides a means of assessing the thickness of a coating.

3.2. Defect detection

At an adhesion defect, the thermal wave reflection coefficient changes from the coating/substrate value to that of the coating/air defect system. The change in phase angle, resulting from the change in reflection coefficient, is shown schematically in Fig. 5b. Thus adhesion defects can be detected by this change in phase angle that they produce.

4. Experimental system

Fig. 6 is a schematic diagram of the experimental

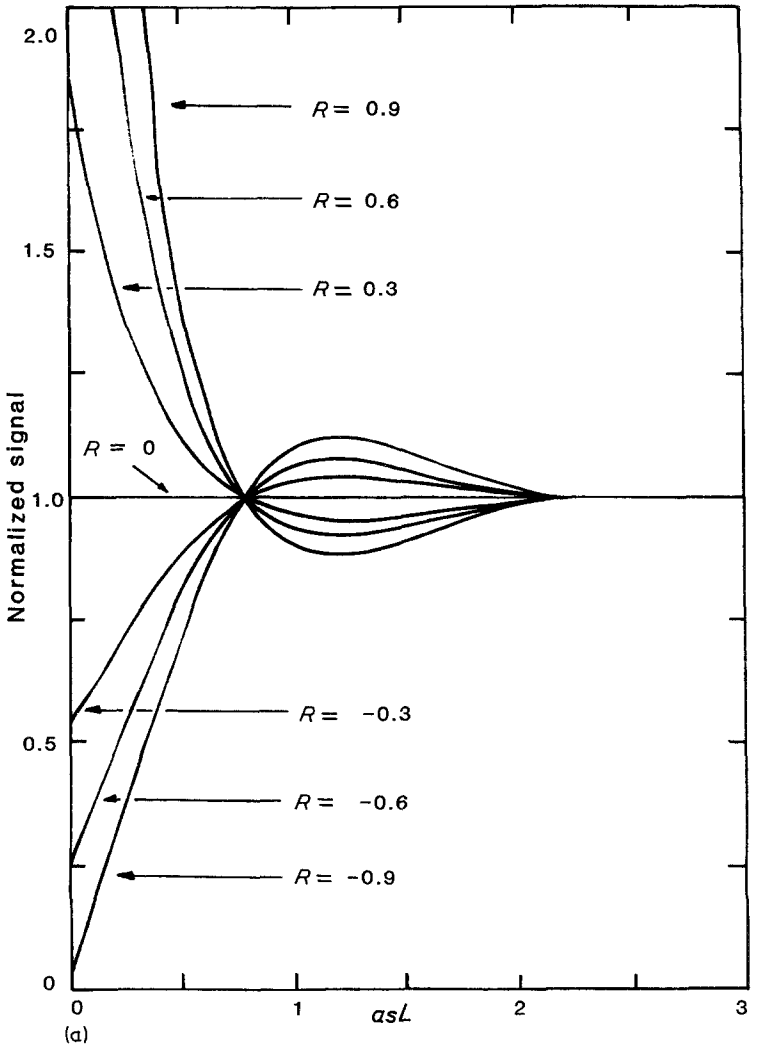

Figure 4 (a) and (b) The variations in the normalized signal and phase angle as a function of the thermal thickness asL, the product of the thermal wave number and the coating thickness, for different interface reflection coefficients R, (adapted from [20]).

system used in this study. The light source was a 5 W argon ion laser (Coherent Innova 90-5) with an unfocused beam diameter of 1 mm at its $1/e$ point. The laser beam was amplitude modulated by a mechanical light chopper (Brookdeal 9479) which provided a workable frequency range of 5 to 800 Hz. An infrared thermal detector (Mullard tri-glycine sulphate) monitored the thermal emissions from the illuminated spot on the sample. A 3 mm thick bloomed (10 μm) germanium lens was used to focus the thermal radiation on to the detector element. The lens also acted as a filter, which was necessary to prevent the reflected laser light reaching the detector element. The detected signal was then processed by a lock-in analyser (EG and G 5206) to monitor the amplitude and phase of the input signal. All data acquisition and sample translation were controlled by a Commodore (PET) 3032 microcomputer.

Three types of samples were prepared to test the predictions of the analysis in Section 3. These samples were:

1. self supporting molybdenum coatings of a variety of thicknesses;

2. stepped thickness coating of nickel aluminide (thicknesses of 15 to 195 μm) sprayed on a 3 mm thick mild steel substrate; and

3. an adhesion defect in an aluminium sprayed coating on a steel substrate.

A fuller description of sample preparation technique is given by Cox [25].

5. Results and discussion

Fig. 7a is a normalized plot of the phase-angle measurements obtained for the self-supporting molybdenum coatings. In these, and the measurements which follow, the normalized phase angle represents the phase shifts associated with thermal

Figure 4 Continued.

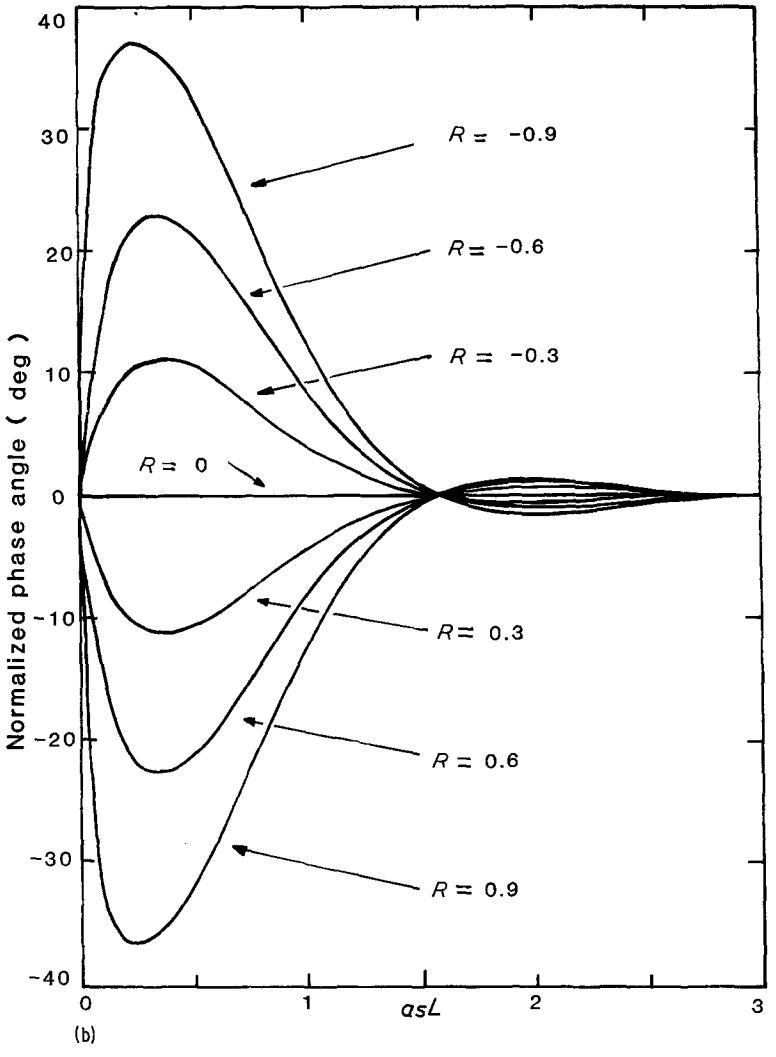

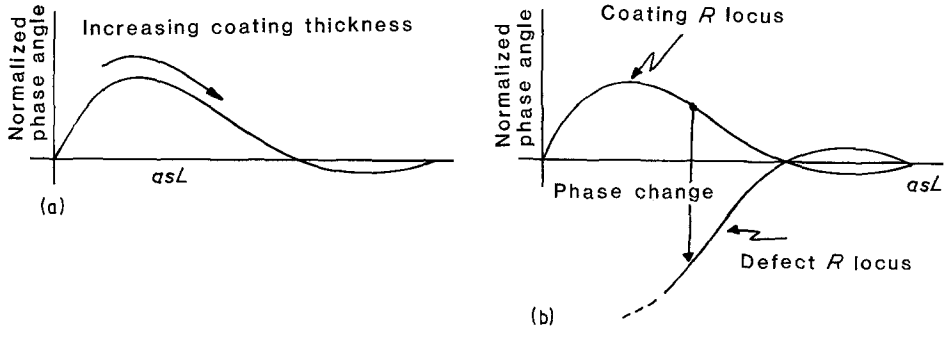

Figure 5 (a) Changes in the normalized phase angle with increasing coating thickness for a particular coating/substrate reflection coefficient R. (b) Schematic illustration of the change in the normalized phase angle at a thermally thick air defect at the coating/substrate interface.

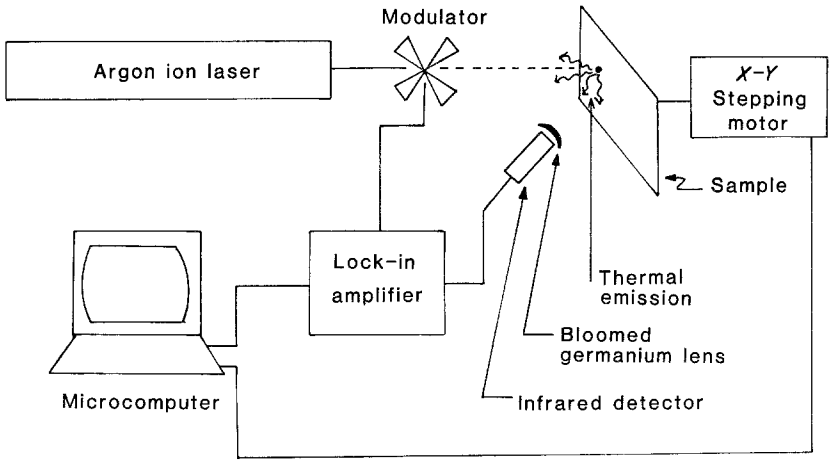

Figure 6 A block diagram of the experimental test system.

wave interference effects in the coating material. This phase angle can be obtained from the experimentally recorded phase angles as shown below:

$$\psi_n = \psi_s - \psi_{ref}, \quad (6)$$

where ψ_s is the experimentally observed phase angle of the test piece and ψ_{ref}, the phase angle recorded by the system for a thermally thick sample ($\mu \ll L$) under the same operating conditions. In this thick sample thermal wave interference effects are absent. The agreement of the experimental data, Fig. 7a, with the theoretical curve, generated using an air-backing reflection coefficient R of 1, is very good. The figure also demonstrates the reduction in thickness resolution with increasing coating thickness. Measurement of coatings of larger thicknesses would necessitate the use of thermal waves of a longer wavelength. These would be produced by using lower modulation frequencies than the 15 Hz used here.

Fig. 7b shows a normalized phase-angle plot of the data obtained for the NiAl stepped coating thickness sample. Again a good fit with theory is obtained. The curve, generated by the parameters listed in the figure, provided the best overall fit to the experimental data. Conventional flash method measurements [26] of thermal conductivity and diffusivity for this coating material are also shown in the figure. The good agreement between the two sets of results shows the potential value of the thermal wave technique for obtaining the thermal properties of the coating materials.

Fig. 7c shows the variation of signal and phase across the adhesion defect, measured at several different chopping frequencies. The presence of the defect can clearly be seen at low modulation frequencies (long thermal wavelengths) in both the signal and phase measurements. The traces indicate the greater sensitivity of phase-angle measurements to the presence of subsurface defects [27, 28]. The defect disappears at 60 Hz in the signal traces but is still present in the phase-angle trace at this frequency, and continues to be present to about 160 Hz. These results also indicate that the depth of a defect below the surface may be determined from its signature at different modulation frequencies [17, 27, 28].

All the above observed phase-angle changes are attributed to thermal wave interference in the coatings. The occurrence of thermal wave interference effects accounts for all the potential advantages of the photothermal method over ultrasonics, as a technique for testing these coatings.

The observations of interference phenomena for thermal waves and their absence for ultrasonic waves shows that the attenuation of thermal waves by coating material is very much lower than that found for ultrasonic waves. To explain this we must consider the propagation of ultrasonic and thermal waves through coating material. Thermal sprayed coatings might be modelled by overlapping layers of coating material separated by thin air gap regions. The arrangement shown in Fig. 8a is a first approximation to this coating structure. A basic structure unit can be identified as that shown in Fig. 8b. Since the layers of coating material are typically 5 to 10 μm, we can make the assumption that both ultrasonic and thermal waves are negligibly attenuated as they travel

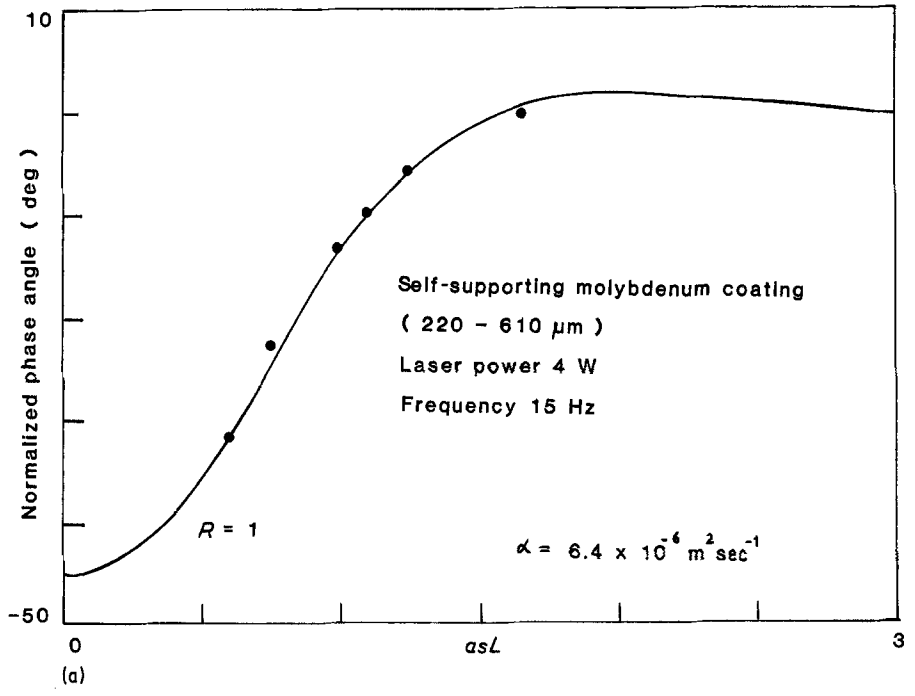

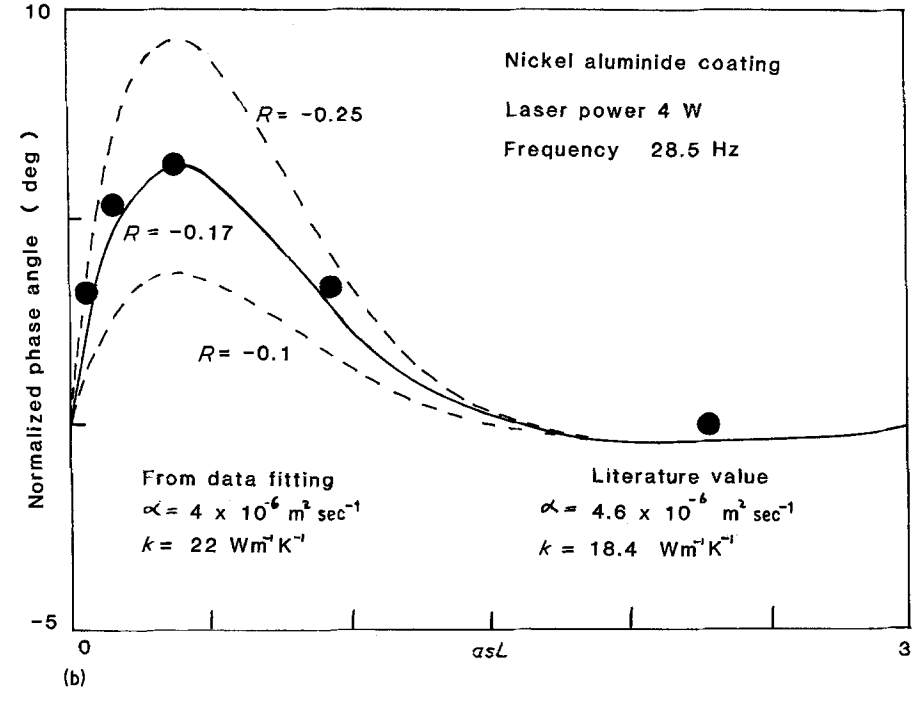

Figure 7 (a) A normalized phase-angle plot of the experimental data (•) against the thermal thickness, asL, for plasma-sprayed self-supporting molybdenum coating of different thicknesses. ——— theoretical curve $R = 1$. (b) A fitting of the experimental data (•) of the normalized phase angle of plasma-sprayed nickel aluminide at 28.5 Hz against thermal thickness. The solid and dashed lines represent the theoretical curves for different R values. (c) The observed signal and phase-angle changes across an adhesion defect for several different modulation frequencies.

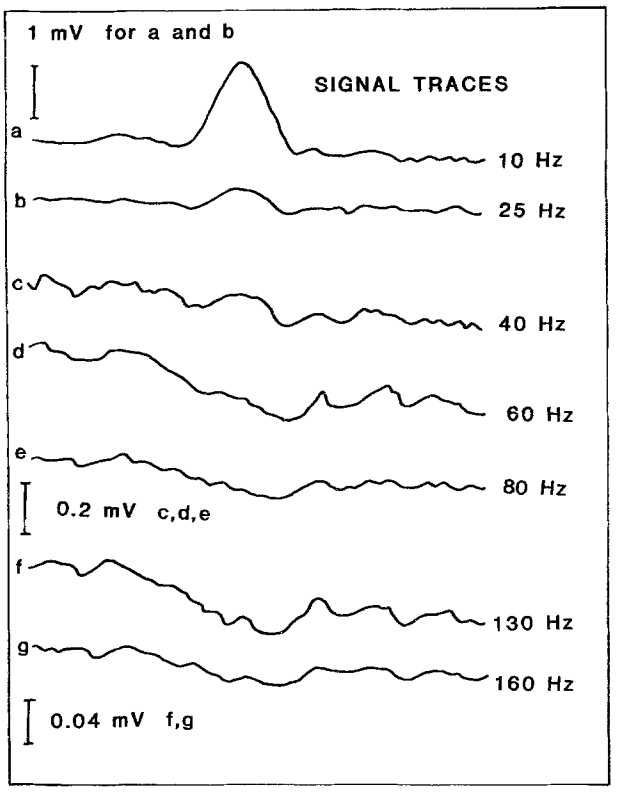

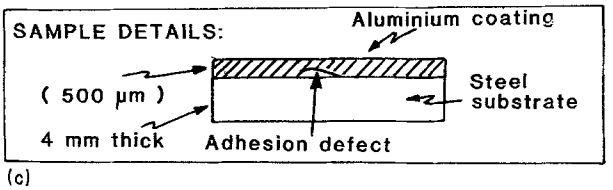

(c)

Figure 7 Continued.

through them. Any attenuation caused by the structure, as a whole, is attributed to transmission losses across the 0.1 μm air gaps.

The sound intensity transmission coefficient, A_t, for the three layer system shown in Fig. 8b, is given by [29]:

$$A_t = \frac{4Z_1Z_2}{(Z_1+Z_3)^2\cos^2 k_2L + [Z_2 + (Z_1Z_3/Z_2)]^2 \sin^2 k_2L} \quad (7)$$

where $Z_i = \rho_i c_i$ is the acoustic impedance of medium i, $(i = 1, 2, 3)$, ρ_i is the density of medium i, c_i the longitudinal wave velocity, k_2 the wave number in medium 2, and L the thickness of medium 2.

Equation 7 can be simplified by making the approximations $Z_1 = Z_3$, $Z_1 \gg Z_2$ and $k_2L \ll 1$ to:

$$(A_t)_{ultra} \approx \frac{1}{1 + (Z_1k_2L/2Z_2)^2}. \quad (8)$$

For thermal waves the equivalent expression for (A_t) can be obtained by taking the square root of the right-hand side of Equation 7, $Z_1 \ll Z_2$ and setting $Z_1 = Z_3$ and $k_2L \ll 1$, as before

$$(A_t)_{thermal} \approx \left\{\frac{1}{1 + (Z_2k_2L/2Z_1)^2}\right\}^{1/2}. \quad (9)$$

This quantity will then represent the amplitude transmission coefficient for these waves. The reason for the first modification to A_t is that in photothermal studies, the amplitude of the thermal waves, the temperature, is monitored rather than the intensity. The reason for the second, that $Z_1 \ll Z_2$ for the thermal waves and $Z_1 \gg Z_2$ for ultrasonic waves, lies in the different definitions of the impedance for the two types of

Figure 7 Continued.

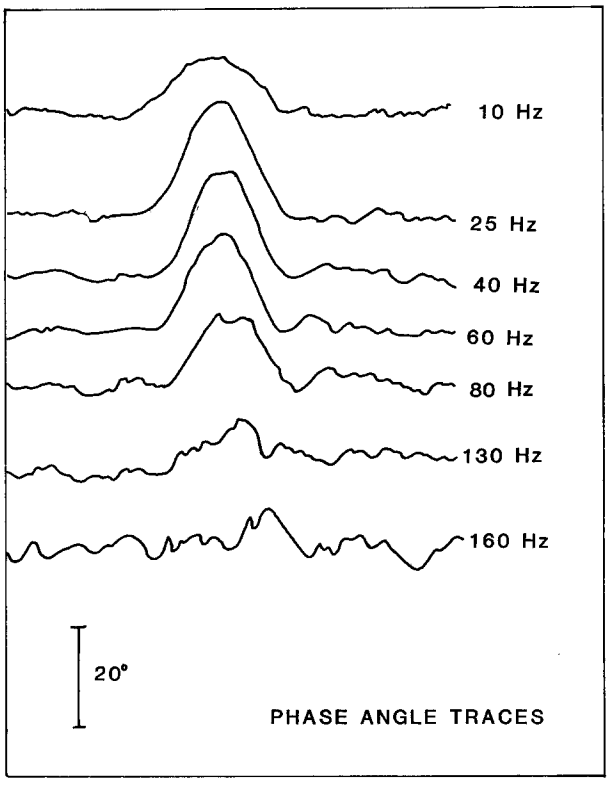

Phase angle depth penetration:

$$= \left(\frac{160}{60}\right)^{1/2} \approx 1.6 \text{ x better than signal}$$

(c)

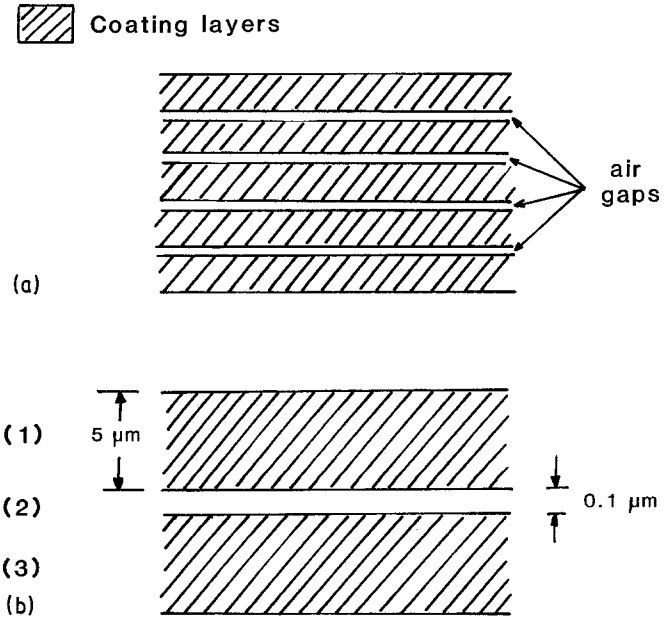

Figure 8 (a) A schematic model of the plasma-sprayed coating built up from an overlapping sequence of coating material and air gap layers. (b) A structural repeat unit of the coating model represented in (a).

TABLE II Experimental and physical parameters for the calculation of the thermal and ultrasonic wave attenuation coefficient for the structure shown in Fig. 8b

Physical and experimental parameters	Thermal	Physical and experimental parameters	Acoustic
Coating thermal impedance ($m^2\,K\,W^{-1}$)	$Z_1 = \frac{1}{k_1\sigma_1} = \frac{1.22\times10^{-5}}{f^{1/2}}(1-j)$	Coating acoustic impedance ($kg\,m^{-2}\,sec^{-1}$)	$Z_1 = \rho_1 c_1 \sim 4\times10^7$
Air gap thermal impedance ($m^2\,K\,W^{-1}$)	$Z_2 = \frac{1}{k_2\sigma_2} = \frac{0.05}{f^{1/2}}(1-j)$	Air gap acoustic impedance ($kg\,m^{-2}\,sec^{-1}$)	$Z_2 = \rho_2 c_2 \sim 4\times10^2$
Air gap thickness (μm)	$L = 0.1$	Air gap thickness (μm)	$L = 0.1$
Thermal wave number of air at 25 Hz (m^{-1})	$k_2 = \left(\frac{\pi f}{\alpha}\right)^{1/2} = 4\times10^2\,25^{1/2}$ $\sim 2\times10^3$	Acoustic wave number of air at 10 MHz (m^{-1})	$k_2 = \frac{2\pi f}{c_2} = \frac{2\pi\times10^7}{4\times10^2}$ $\sim 1.6\times10^5$
$\frac{Z_2}{Z_1}$	$\frac{5\times10^{-2}}{1.22\times10^{-5}} \sim 4\times10^3$	$\frac{Z_1}{Z_2}$	$\frac{4\times10^7}{4\times10^2} \sim 10^5$
k_2L	$(2\times10^3)\times10^{-7} \sim 2\times10^{-4}$	k_2L	$(1.6\times10^5)\times10^{-7} \sim 1.6\times10^{-2}$
$(A_t)_{thermal} = \left[\frac{1}{1+(Z_2k_2L/2Z_1)^2}\right]^{1/2} \approx 0.93$		$(A_t)_{ultrasonic} = \frac{1}{1+(Z_1k_2L/2Z_2)^2} \approx 10^{-6}$	

wave. For thermal waves thermal impedance is defined as [16]:

$$Z = 1/k\sigma = (1-j)(4\rho Ck\pi f)^{-1/2},$$

where ρ, C and k are the density, heat capacity and thermal conductivity of the medium and f is the frequency of the thermal wave. This expression can be derived by the direct analogy of the temperature and heat flux with electric potential and current. Physically, this means that for a low thermal conductivity medium, such as air, the thermal impedance is large. This contrasts with the acoustic impedance which is small for such a low density medium.

Table II summarizes the necessary data for the evaluation of A_t, for typical coating parameters and experimental conditions. The wave numbers shown are for the 25 Hz thermal waves and 10 MHz ultrasonic waves [30] that have been found to be suitable for testing these coatings. It can be seen from this table that ratios of impedances (Z_2/Z_1 or Z_1/Z_2), which appear in the thermal and acoustic expressions for A_t, differ by about two orders of magnitude. Similarly the wave numbers, for the two types of wave in the air gaps, differ by about two orders of magnitude whereas they are of similar magnitude in the solid layers. The combination of these two effects results in the terms in the denominators of the expressions for A_t, being large for ultrasonic waves and small for thermal waves. As a consequence, the same structural unit is found to be highly attenuating for ultrasonic waves but virtually transparent for thermal waves.

The above analysis indicates that a 0.1 μm air gap would account for about 60 dB of ultrasonic attenuation. This amounts to an attenuation of 60 000 dB for a centimetre thickness of coating material consisting of a stack of the 10 μm structural units of the type shown in Fig. 8b. This figure is two orders of magnitude larger than the values of 500 dB cm^{-1} reported by Cox *et al.* [2, 30]. This can be attributed to the obvious deficiency in our simple model of an absence of contact between layers of coating material. Such contacts must be present to hold the coating together and are clearly evident in SEM studies of coating material (see references in Table I). These contacts will, of course, reduce the attenuation from the maximum levels calculated here. It would be difficult to modify our model to incorporate the effects of the multiple contacts between layers found in real coating material. However, we believe that the model accounts, in principle, for the simultaneous very high ultrasonic attenuation and apparent transparency of coating material to thermal waves. Although this sensitivity of thermal waves to air gaps facilitates thermal wave interferometry for coating thickness determination; it also leads to a comparative insensitivity to the presence of sub-micron width adhesion defects at the coating/substrate interface.

This work has shown that low-frequency thermal waves offer significant advantages to

ultrasonic waves for the penetration of materials consisting of stratified media. The advantages originate in the difference in the fundamental mechanisms which govern the propagation of the two types of waves. It has been shown that a thin air layer can be simultaneously highly attenuating to ultrasonic waves and virtually transparent to thermal waves. This facilitates the quantitative study, by thermal wave interferometry, of materials which present practical problems to established ultrasonic techniques. The technique is non-contactive and has been demonstrated to determine the thickness, the presence of defects and the thermal properties of a variety of plasma-sprayed coatings.

Acknowledgement

This work was supported by grants from the Science and Engineering Research Council, UK.

References

1. R. C. TUCKER JR, in "Deposition technologies for films and coatings", edited by R. F. Bunshah (Noyes Publication, New Jersey, USA, 1982).
2. R. L. COX, D. P. ALMOND and H. REITER, *Ultrasonics* **19** (1981) 17.
3. D. R. GREEN, *J. Appl. Phys.* **37** (1966) 3095.
4. M. V. LUUKKALA, "Scanned image microscopy", edited by E. A. Ash (Academic Press, London, 1980) p. 273.
5. G. BUSSE and P. EYERER, *Appl. Phys. Lett.* **43** (1983) 535.
6. N. N. AULT, *J. Amer. Ceram. Soc.* **40** (1957) 69.
7. T. B. BUZOVKINA, T. V. SOKOLOVA, A. P. OBUKHOV, R. I. USPENSKAGA and M. G. DEGEN, *High Temp. (USA)* **10** (1972) 345.
8. S. SAFAI and H. HERMAN, Proceedings of the International Conference on Advances in Surface Coatings Technology, February 13–15, 1978, London (The Welding Institute, 1978) Paper 5.
9. R. MCPHERSON and B. V. SHAFER, *Thin Solid Films* **97** (1982) 201.
10. V. WILMS and H. HERMAN, *ibid.* **39** (1976) 251.
11. S. SAFAI and H. HERMAN, *ibid.* **45** (1977) 295.
12. J. B. KINNEY and R. H. STALEY, *Ann. Rev. Mat. Sci.* **12** (1982) 295.
13. Y. H. WONG, in "Scanned image microscopy", edited by E. A. Ash (Academic Press, London, 1980) p. 247.
14. A. J. ANGSTROM, *Ann. Phys. (Leipzig)* **114** (1861) 513.
15. L. VERENI and A. SANTUCCI, *Il Nuovo Cimento B (Italy)* **62B** Ser 2 (1981) 399.
16. H. S. CARSLAW and J. C. JAEGER, "Conduction of heat in solids" (Clarendon Press, Oxford, 1959) pp. 64–9.
17. D. R. GREEN, *Mat. Eval. (USA)* **25** (1967) 231.
18. J. OSPAL and A. ROSENCWAIG, *J. Appl. Phys.* **53** (1962) 4240.
19. F. ALAN MCDONALD, *Amer. J. Phys.* **48** (1980) 41.
20. C. A. BENNET JR and R. R. PATTEY, *Appl. Opt.* **21** (1982) 45.
21. R. L. THOMAS, L. D. FAVRO, K. R. GRICE, L. J. INGLEHART, P. K. KUO, J. LHOTA and G. BUSSE, *IEEE Ultrasonics Symp.* **2** (1982) 586.
22. M. LUUKKALA, A. LETHO, J. JAHRINEN and M. JOKINEN, *ibid.* **2** (1982) 591.
23. P. -E. NORDAL and S. O. KANSTAD, *Phys. Scr.* **20** (1979) 659.
24. G. BUSSE, *Infrared Phys.* **20** (1980) 419.
25. R. L. COX, MSc thesis, University of Bath (1979) unpublished.
26. J. DANIAULT, J. de GOER and G. SCHNEDEKER, Preprints of 8th International Thermal Spraying Conference, September, 1976, Florida, USA (American Welding Society) p. 310.
27. R. L. THOMAS *et al.*, *J. Appl. Phys.* **51** (1980) 1152.
28. G. BUSSE and A. ROSENCWAIG, *Appl. Phys. Lett.* **36** (1980) 815.
29. W. W. SETO, "Theory and problems in acoustics", Schaum's outline series (McGraw Hill, 1971) p. 99.
30. R. L. COX, D. P. ALMOND and H. REITER, *NDT Int.* **13** (1980) 291.

Received 19 March
and accepted 16 May 1984